

ISAR Multi-band Fusion Based on Attributed Scattering Center

Yu Ning Feng Zhou* Lei Liu

The Ministry Key Laboratory of Electronic Information
Countermeasure and Simulation
Xidian University
Xi'an, China

Xueru Bai

National Laboratory of Radar Signal Processing
Xidian University,
Xi'an, China
fzhou@mail.xidian.edu.cn

Abstract—High resolution Inverse synthetic aperture radar imaging is an important technique for aerospace targets recognition. Multi-band fusion method greatly improves the radar bandwidth without the increasing of hardware cost. Traditional Multi-band fusion methods usually adopt damped exponential model or geometrical theory of diffraction model, but these models are not precise enough, especially when the target is complex. This paper proposes a novel multi-band fusion method based on attributed scattering center model. Firstly, The ASCs of different subbands are extracted using zoom dictionary; Secondly, the vacant band is recovered; Finally, the coherence phase is compensated, and the full-band signal is obtained. Compared with traditional methods, the proposed method has higher range resolution.

Keywords — Inverse synthetic aperture radar; Multi-band Fusion; Attributed scattering center

I. INTRODUCTION

Inverse synthetic aperture radar (ISAR) imaging is a significant approach to classify, recognize and surveillance aerospace targets. The range resolution is a key indicator of ISAR imaging. A directly approach to improve range resolution is increasing the bandwidth. However, it brings huge burden on hardware cost. An alternative method is to utilize several radars working in different frequencies [1]. After coherent processing, integrated wideband signal is obtained. The essence of multi-band fusion is extrapolating the vacant band between measurement subbands. Traditional multi-band fusion methods can be classified into two categories. The first category is non-parametric methods, which require no prior information of targets. [2] proposes the amplification gapped-data amplitude and phase estimation (GAPES) method. This method adopts least-squares (LS) technique to iteratively estimate the unknown frequency spectrum. Simulation and measured data confirm its efficiency, but improper initialization may let the method drop into local optima. [3] models the phase deviations of different radars as linear phase and constant phase. This method employs

all-phase fast Fourier transform (apFFT) to estimate the constant phase and estimates the linear phase by correlating the images after pulse compression. Then iterative adaptive approach (IAA) is performed to fuse multi-band signal.

The second category is parametric methods, which establish parametric models and solve relevant parameters. Compared with non-parametric methods, parametric methods employ rich prior information and have more excellent performance. According to the model adopted, these methods can be classified to two subclasses. The first subclass is based on damped exponential (DE) model. [5] proposes a multi-band fusion method based on all-pole model. This method builds forward-prediction matrices for lower and upper subbands, respectively. Then, singular-value decomposition and Akaike information criterion are adopted to estimate the number of poles and LS technique is adopted to solve model parameters. After compensating phase offset, the integrated frequency signal is gained. However, this method is hard to determine the model-order in low signal to noise ratio (SNR). The second subclass employs geometrical theory of diffraction (GTD) model. [6] combines two measurement bands, and constructs a frequency dictionary to estimate back-scattering coefficients using fast sparse Bayesian learning algorithm. Making use of back-scattering coefficients and full-band dictionary, the integrated band signal is recovered. Moreover, dynamic dictionary decreases the computing burden.

Even though those methods aforementioned have well performance in some situations, the range resolution is restricted by the precision of DE model and GTD model, especially when the target is complex. This paper models the target using more precise attributed scattering center (ASC) model [7], and zoom dictionary is adopted to extract ASCs of different subbands. We elaborately deduce the origin of coherence phase and utilize genetic algorithm (GA) to calculate it. After compensating the coherence phase, the integrated wideband signal is obtained.

The remainder of this paper is organized as follows. Section II derives multi-band signal fusion model. Section III introduces the ASC model and the extraction method. Section IV shows the means of compensating coherence phase between different subbands. Section V presents the fusing results and analyzes the performance of the proposed method. Section VI concludes the paper.

This work was supported in part by the National Natural Science Foundation of China under Grant No. 61201283, No. 61471284, No. 61522114, 612310107 and by the NSAF under Grant No. U1430123; it was also supported by the Foundation for the Author of National Excellent Doctoral Dissertation of P.R. China under Grant No. 201448, and by Program for New Century Excellent Talents in University under Grant NCET-12-0916. This work was supported by the Fundamental Research Funds for the Central Universities under Grant No. KJXX1601, No. 7214534206 and the Young Scientist Award of Shaanxi Province under Grant No. 2015KJXX-19 and 2016KJXX-82. This work was supported by the Postdoctoral Science Foundation of China under Grant 2016M602775 and 2017M613076.

II. MULTI-BAND SIGNAL FUSION MODEL

Echoes of several radars working in different frequencies can be composed into a wideband signal which has wider bandwidth. Without loss of generality, this paper takes two radars as an example, and more radars are similar.

Supposing two radars are located at S and S' , as shown in Fig. 1, the radar coordinate system of radar1 is (U, V, W) with origin S . The radar coordinate system of radar2 is (U', V', W') with origin S' . In (U, V, W) , the distance between the target and radar1 is L_1 . In (U', V', W') , the distance between the target and radar1 is L_2 . Because the distance between the radar and the target is much larger than the distance between two radars, i.e. $SS' \ll L_1$ and $SS' \ll L_2$. Thus, $\overline{SP} \approx \overline{S'P}$. P is any scatterer of target.

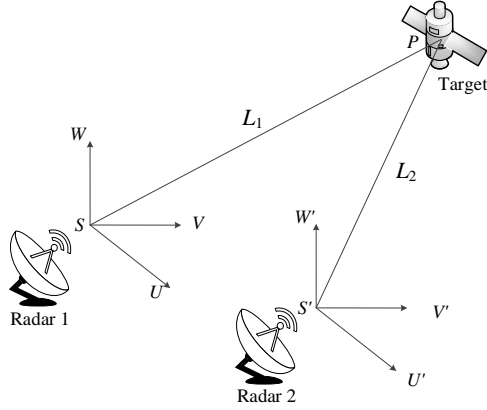


Fig. 1 Multi-band signal fusion model.

Assuming that two radars transmit pulse signal with the same period T_p , the time of transmitting is $t_m = mT$ ($m = 0, 1, \dots$), which is called as slow time. Fast time \hat{t} corresponds to the propagation time of electromagnetic waves, and $t = \hat{t} + mT$. The transmitted linear frequency modulation (LFM) signal is expressed as

$$s_{kr}(\hat{t}, t_m) = \text{rect}\left(\frac{\hat{t}}{T_p}\right) \cdot \exp\left(j2\pi\left(f_{kc}t + \frac{1}{2}\gamma\hat{t}^2\right)\right) \quad (1)$$

where $k=1, 2$, and k is the k^{th} radar, and $\text{rect}(t) = 1, \text{only if } |t| \leq 1/2$, and f_{kc} is central frequency of k^{th} radar, and T_p is the pulse width. γ denotes the chirp acceleration term of an LFM waveform. For simplicity of formula derivation, two radars transmit signals of same waveform only with different frequencies. In fact, sample frequency, pulse width and chirp acceleration term may be different. However, interpolation processing is able to handle this problem.

Assuming that the first-order Born approximation is satisfied, the target consists of L scatterers. Echoes of k^{th} radar can be expressed as

$$s_{kr}(\hat{t}, t_m) = \sum_{l=1}^L \rho_{kl} \text{rect}\left(\frac{\hat{t} - 2R_{kl}(t)/c}{T_p}\right) \cdot \exp\left(j2\pi\left(f_{kc}(t - 2R_{kl}(t_m)/c) + \frac{1}{2}\gamma(\hat{t} - 2R_{kl}(t_m)/c)^2\right)\right) \quad (2)$$

where $R_{kl}(t)$ is the instant distance between the l^{th} scatterer and the k^{th} radar, and ρ_{kl} is the back-scattering coefficient of the l^{th} scatterer in the k^{th} radar. De-chirping processing is performed to compress pulse. Let the references range of two radars are all R_{ref} , and the reference signal is shown in (3).

$$s_{ref}(\hat{t}, t_m) = \text{rect}\left(\frac{\hat{t} - 2R_{ref}(t)/c}{T_{ref}}\right) \cdot \exp\left(j2\pi\left(f_{kc}(t - 2R_{ref}/c) + \frac{1}{2}\gamma(\hat{t} - 2R_{ref}(t)/c)^2\right)\right) \quad (3)$$

where T_{ref} is the pulse width of reference signal. Let $R_{\Delta kl} = R_{kl}(t) - R_{ref}$, and de-chirping processing is

$$s_{kif}(\hat{t}, t_m) = s_{kr}(\hat{t}, t_m) \cdot s_{ref}^*(\hat{t}, t_m) \quad (4)$$

The difference frequency output of k^{th} radar s_{kif} is

$$s_{kif}(\hat{t}, t_m) = \sum_{l=1}^L \rho_{kl} \text{rect}\left(\frac{\hat{t} - 2R_{kl}(t)/c}{T_p}\right) \cdot \exp\left(-j\frac{4\pi}{c}\gamma\left(\hat{t} - \frac{2R_{ref}}{c}\right)R_{\Delta kl} - j\frac{4\pi}{c}f_{kc}R_{\Delta kl} + j\frac{4\pi\gamma}{c^2}R_{\Delta kl}^2\right) \quad (5)$$

Due to $\overline{SP} \approx \overline{S'P}$, $R_{1l}(t) \approx R_{2l}(t)$ is appropriate in envelope, and it is simplified as $R_l(t)$. However, the phase is much more sensitive to range bias than the envelope, so $R_{1l}(t) \neq R_{2l}(t)$ in the phase. Phase term $\exp\left(-j\frac{4\pi}{c}f_{kc}R_{\Delta kl} + j\frac{4\pi\gamma}{c^2}R_{\Delta kl}^2\right)$ is independent of time, and it is simplified as $\exp(j\phi_k)$. Thus, (5) is rewritten as

$$s_{kif}(\hat{t}, t_m) = \sum_{l=1}^L \rho_{kl} \text{rect}\left(\frac{\hat{t} - 2R_l(t)/c}{T_p}\right) \cdot \exp\left(-j\frac{4\pi}{c}\gamma\left(\hat{t} - \frac{2R_{ref}}{c}\right)R_{\Delta kl} + j\phi_k\right) \quad (6)$$

The difference of the de-chirped echoes of two radars is

$$s_{if}(\hat{t}, t_m) = \sum_{l=1}^L \rho_{kl} \text{rect}\left(\frac{\hat{t} - 2R_l(t)/c}{T_p}\right) \cdot \exp\left(-j\frac{4\pi}{c}\gamma\left(\hat{t} - \frac{2R_{ref}}{c}\right)R_{\Delta l} + j\Delta\phi\right) \quad (7)$$

where $R_{\Delta l} = R_{1l}(t) - R_{2l}(t)$, $\Delta\phi = \phi_1 - \phi_2$. Simplify the phase of (7), and the phase difference $\Delta\Phi$ is as shown in (8).

$$\Delta\Phi = \exp\left(-j\frac{4\pi}{c}\gamma R_{\Delta l} \hat{t} + j\frac{8\pi R_{ref}}{c^2}\gamma R_{\Delta l} + j\Delta\phi\right) \quad (8)$$

(8) reveals that the phase difference consists of linear phase and constant phase, i.e.

$$\Delta\Phi = \exp(j\lambda\hat{t} + j\tau) \quad (9)$$

where $\lambda = -\frac{4\pi}{c}\gamma R_{\Delta}$, $\tau = \frac{8\pi R_{ref}}{c^2}\gamma R_{\Delta} + \Delta\phi$.

In order to figure out the coherent phase, it is necessary to represent the signals as precise as possible. Traditional DE model and GTD model are no more appropriate, so ASC model is introduced in this paper.

III. ATTRIBUTED SCATTERING CENTER MODEL AND EXTRACTION TECHNIQUE

The ASC model [7] is proposed on the base of GTD model. The response of the i^{th} ASC is

$$E_i(f, \phi; \theta) = A_i \left(j \frac{f}{f_c} \right)^{\alpha_i} \exp \left(-j \frac{4\pi f}{c} (x_i \cos \phi + y_i \sin \phi) \right) \cdot \text{sinc} \left(\frac{2\pi f}{c} L_i \sin(\phi - \bar{\phi}_i) \right) \exp(-2\pi f \gamma_i \sin \phi) \quad (10)$$

where A_i denotes the backscattered coefficient, α_i the frequency dependence, f the radar frequency, f_c the central frequency, ϕ the cross-range angle, x_i and y_i the range and cross-range locations, respectively. The remaining three parameters $\bar{\phi}_i$, L_i and γ_i determine the aspect dependence of the scattering. According to these parameters, ASCs are classified into localized ASCs and distributed ASCs.

Compared with DE model and GTD model, ASC model is more precise but its extraction technique is more complex. Conventional extraction techniques are classified into image-domain methods and frequency-domain methods. Image-domain methods extract ASCs in image domain after decoupling, but distributed ASCs may be divided into several localized ASCs by mistake. Frequency-domain methods construct dictionaries based on signal model and calculate the best reconstruction by Orthogonal Matching Pursuit (OMP). However, huge dictionaries need a lot of resources. In order to solve these problems, zoom dictionary extraction technique [8] is adopted. The signal can be rewritten as

$$\mathbf{s} = \mathbf{D}(\theta) \boldsymbol{\sigma} \quad (11)$$

where \mathbf{s} is the vectorization of measurements $E(f, \phi; \theta)$ \mathbf{D} is a redundant dictionary, and $\boldsymbol{\sigma}$ is a complex sparse vector whose element denotes the backscattering amplitude.

$$D(x, y, L, \bar{\phi}) = [\bar{d}_1, \bar{d}_2, \dots, \bar{d}_{n-1}, \bar{d}_n] \quad (12)$$

where $\bar{d}_i = d_i / \|d_i\|_2$ and d_i is a combination of parameters as shown in (13)

$$d_i = \exp \left(\frac{-j4\pi f}{c} (x_i \cos \phi + y_i \sin \phi) \right) \cdot \text{sinc} \left(\frac{2\pi f}{c} (L_i \sin(\phi - \bar{\phi}_i)) \right) \quad (13)$$

To reduce computation load, the scopes of x , y , L and $\bar{\phi}$ should be as small as possible. We need to determine these parameters using prior information as shown below.

$$x \in [x_{\min}, x_{\max}], y \in [y_{\min}, y_{\max}], L \in [0, L_{\max}], \bar{\phi} \in [\phi_1, \phi_2] \quad (14)$$

After the scope is determined, OMP algorithm is applied to solve parameters. However, high precise result requires a huge dictionary, and zoom dictionary is adopted to mitigate this contradiction. A huge spaced dictionary is constructed to calculate parameters coarsely. Then, a refined dictionary is constructed to obtain precise results. The gap of huge spaced dictionary is set as radar resolution, and the result is as precise as the resolution. Supposing the result of the i^{th} iteration is $x_i, y_i, L_i, \bar{\phi}_i$, the scopes of refined dictionary are shown below.

$$x \in \left[x_i - \frac{t_x}{2}, x_i + \frac{t_x}{2} \right], y \in \left[y_i - \frac{t_y}{2}, y_i + \frac{t_y}{2} \right] \quad (15)$$

$$L \in \left[L_i - \frac{t_L}{2}, L_i + \frac{t_L}{2} \right], \bar{\phi} \in \left[\bar{\phi}_i - \frac{t_{\bar{\phi}}}{2}, \bar{\phi}_i + \frac{t_{\bar{\phi}}}{2} \right] \quad (16)$$

where t_x, t_y, t_L and $t_{\bar{\phi}}$ are the gaps of huge spaced dictionary. After the refined extraction, precise result is gained.

With x_i, y_i, L_i and $\bar{\phi}_i$, the rest parameters α_i and γ_i can be estimated easily. Finally, A_i is obtained by LS criterion. The flow of ASC extraction algorithm is shown in TABLE 1

TABLE 1 FLOW OF ASC EXTRACTION ALGORITHM

Step1: Construct huge spaced dictionary $D_1(x, y)$ and $D_2(L, \bar{\phi})$;
Step2: Calculate coarse $x, y, L, \bar{\phi}$ using OMP;
Step3: According to the coarse result, Construct refined dictionary $D_3(x, y)$ and $D_4(L, \bar{\phi})$;
Step4: Calculate refined $x, y, L, \bar{\phi}$ using OMP;
Step5: Construct dictionary D_α, D_γ to figure out α and γ , then calculate A using LS;
Step6: Calculate the residual energy Δ . If Δ is smaller than threshold η , the algorithm stops. If not, go to Step2.

IV. MULTI-BAND COHERENT PROCESSING

Before multi-band signals are fused, coherent processing is necessary. The ASC extractions of lower subband and upper subband are expressed as $E_p(f, \phi; \theta)$ and $E_Q(f, \phi; \theta)$, respectively. We extrapolate the lower subband and upper subband and obtain overlapped subband as indicated in Fig. 2.

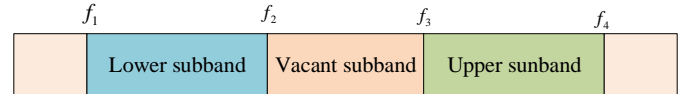


Fig. 2 Multi-band signal extrapolation.

The extrapolation subbands of lower subband and upper subband are expressed as (17) and (18), respectively.

$$E_p(f, \phi; \theta) = \sum_{i=1}^{N_p} A_{p_i} \left(j \frac{f_U}{f_{p_c}} \right)^{\alpha_{p_i}} \exp \left(-j \frac{4\pi f_U}{c} (x_{p_i} \cos \phi + y_{p_i} \sin \phi) \right) \cdot \text{sinc} \left(\frac{2\pi f_U}{c} L_{p_i} \sin(\phi - \bar{\phi}_{p_i}) \right) \exp(-2\pi f \gamma_{p_i} \sin \phi) \quad (17)$$

$$E_Q(f, \phi; \theta) = \sum_{i=1}^{N_Q} A_{Q_i} \left(j \frac{f_V}{f_{Q_c}} \right)^{\alpha_{Q_i}} \exp \left(-j \frac{4\pi f_V}{c} (x_{Q_i} \cos \phi + y_{Q_i} \sin \phi) \right) \cdot \text{sinc} \left(\frac{2\pi f_V}{c} L_{Q_i} \sin(\phi - \bar{\phi}_{Q_i}) \right) \exp(-2\pi f \gamma_{Q_i} \sin \phi) \quad (18)$$

where $f_U = [f_1, f_3]$, $f_V = [f_2, f_4]$ and the subscript P and Q denote the lower subband and upper subband, respectively. Let E_U and E_V indicate the lower subband signal and upper subband signal between $[f_2, f_3]$, respectively. According to (9), there exist linear phase λ and constant phase τ between E_U and E_V . On the basis of E_V , we need to minimize the cost function J

$$J = \min_{\lambda, \tau} \sum_{i=f_2/\gamma}^{f_3/\gamma} |E_V - A^* \cdot E_U \cdot \exp(j\lambda i + j\tau)| \quad (19)$$

where A^* is the amplify difference between E_U and E_V . A^* can be solved by normalization but λ and τ should be found by other approaches. Genetic algorithm (GA) [9] is an effective method compared with traversal search. With coherence phase and amplification, lower subband and upper subband are coherent. Then, ASCs of linked full band are extracted and full band signal are obtained. The flowchart of multi-band fusion based on ASC is shown in Fig. 3.

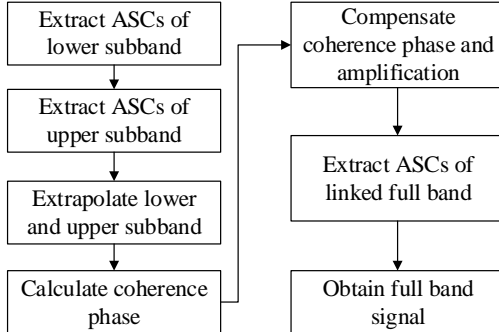


Fig. 3 The flowchart of multi-band fusion based on ASC model.

V. EXPERIMENTS AND ANALYSIS

The first experiment adopts 10 simulated ASCs with radar work frequency 9.5 GHz~12.5 GHz. The known lower subband is 9.5 GHz~10.5 GHz and the known upper subband is 11.5 GHz ~12.5 GHz. linear phase $\lambda = \pi/8$ and constant phase $\tau = \pi/4$ are added to lower subband. The ASCs extraction results are shown in Fig. 4.

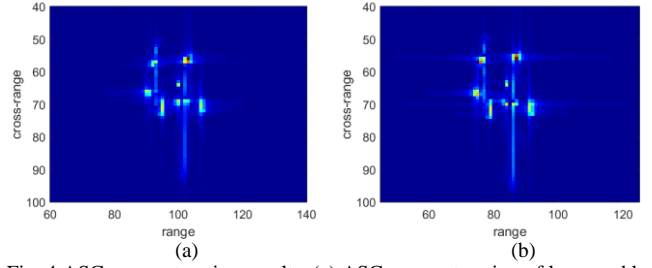


Fig. 4 ASCs reconstruction results. (a) ASCs reconstruction of lower subband (b) ASCs reconstruction of upper subband.

From Fig. 4, it can find that there is offset in range between lower subband and upper subband. The reason is that linear phase in frequency domain leads to position offset in image domain. We take 36th echo as an example, the real part of the signal is demonstrated in Fig. 5 (a). GA is adopted to figure out the coherence phase and the compensated signal is shown in Fig. 5 (b). Upper subband and lower subband is well coherent.

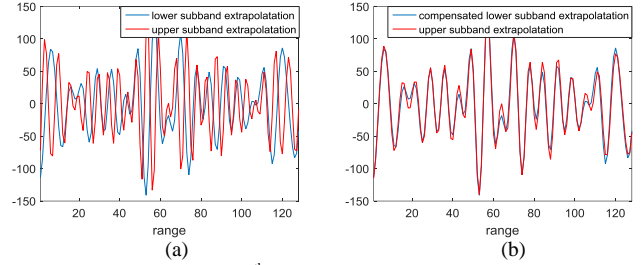


Fig. 5 The real part of the 36th echo. (a) Before coherence phase compensation (b) After coherence phase compensation.

The full band 9.5 GHz~12.5 GHz fusion result is shown in Fig. 6 (b). we compare fusion result with full band signal and the maximum relative error of all the pixels is about 0.1. Because the reconstruction is quite similar with the real target, the result is very well.

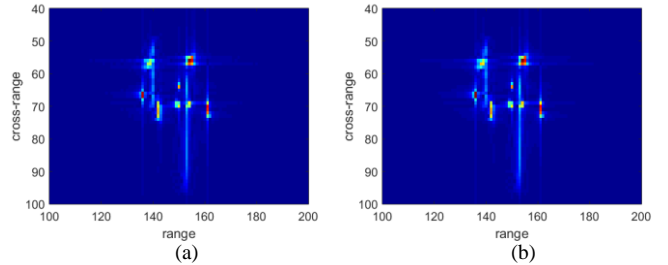


Fig. 6 Multi-band fusion result. (a) True full band signal (b) Fusion result of full band.

In order to confirm the proposed method further, we use a plane electromagnetic data. The plane model is 16.2 m length and 17.7 m width and 3 m height, as shown in Fig. 7.

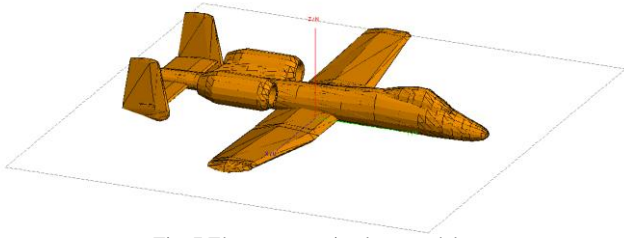


Fig. 7 Electromagnetic plane model.

Lower subband is 10 GHz~11 GHz and upper subband is 12 GHz~13 GHz. Gaussian white noise is added in this experiment with SNR=10 dB. Linear phase $\lambda = \pi/8$ and constant phase $\tau = \pi/4$ are added to lower subband. The ASCs extraction result of lower subband and upper subband are shown in Fig. 8 (b) and (d), respectively. From Fig. 8, it is significant that the main structure of the plane is extracted and the noise is suppressed.

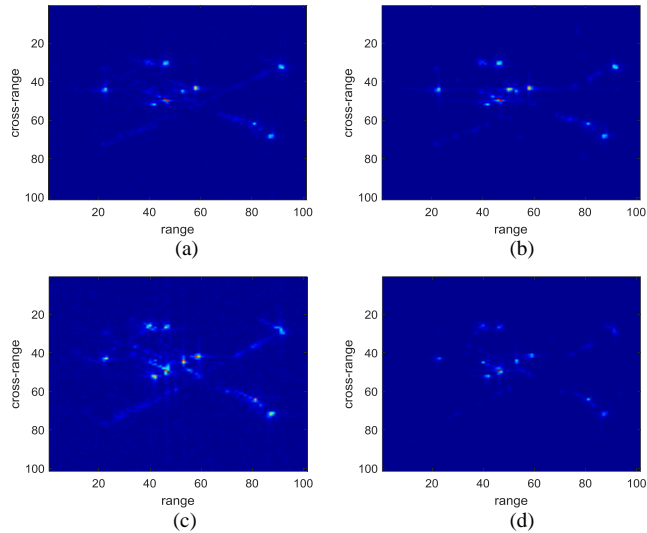


Fig. 8 ASCs extraction results of plane model. (a) Original imaging result of lower subband using FFT (b) ASCs reconstruction of lower subband (c) Original imaging result of upper subband using FFT (d) ASCs reconstruction of upper subband.

After the ASCs are extracted, coherence phase is solved using GA. We adopt polar format algorithm (PFA) to image, and the imaging result of multi-band fusion is shown in Fig. 9 (c). As contracts, PFA imaging results of lower subband and upper subband are shown in Fig. 9 (a) and (b), respectively.

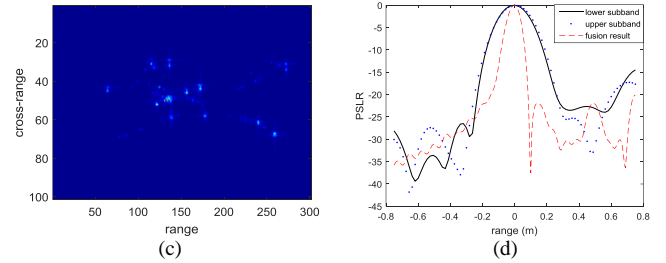
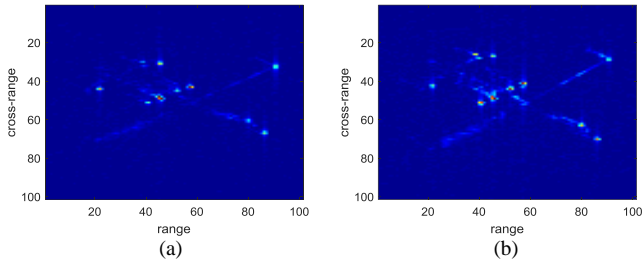


Fig. 9 Imaging results of multi-band fusion using PFA. (a) Imaging result of lower subband (b) Imaging result of upper subband (c) Imaging result of multi-band fusion (d) PSLF of the 52nd cross-range cell.

For measurable analysis, the peak side lobe ratio (PSLR) of the 52nd cross-range cell is drawn in Fig. 9 (d). It is observed that the resolution in range is improved from 0.225 m to 0.08 m (with Hamming window). Additional, conventional method based on DE model and GTD model are unproductive in face of such complex targets.

CONCLUSION

This paper proposes a novel multi-band fusion method based on ASC model other than traditional DE model and GTD model. First, The ASCs are extracted in different bands based on zoom dictionary; Secondly, the vacant band is recovered by extrapolation; Finally, coherence phase is figured out, and the coherent full band is obtained. Compared with traditional methods, the proposed method has higher range resolution, especially in complex situations. The simulation and electromagnetic data confirm the efficiency of the proposed method.

ACKNOWLEDGMENT

The authors would like to thank the anonymous reviewers for their valuable comments and helpful advices.

REFERENCES

- [1] X. Bai, F. Zhou, Q. Wang, M. Xing and Z. Bao, "Sparse Subband Imaging of Space Targets in High-Speed Motion," *IEEE Trans. Geosci. Remote Sens.*, vol. 51, no. 7, pp. 4144-4154, Jul. 2013.
- [2] E. G. Larsson, P. Stoica, and J. Li, "Amplitude Spectrum Estimation for Two-Dimensional Gapped Data," *IEEE Trans. Signal Processing*, vol. 50, no. 6, pp. 1343-1354, Jun. 2002.
- [3] J. Tian, J. Sun, G. Wang, Y. Wang *et al.*, "Multiband Radar Signal Coherent Fusion Processing With IAA and apFFT," *IEEE Signal Process. Lett.*, vol. 20, no. 5, pp. 463-466, May 2013.
- [4] Y. Zheng, S. Tseng and K. Yu, "Spectral Analysis of Periodically Gapped Data," *IEEE Trans. Aerosp. Electron. Syst.*, vol. 39, no. 3, pp. 1089-1097, Jul. 2003.
- [5] K. M. Cuomo, J. E. Piou, and J. T. Mayhan, "Ultra-Wideband Coherent Processing," *The Lincoln Laboratory Journal*, vol. 10, no. 2, pp. 203-222, 1997.
- [6] H. Zhang and R. Chen, "Coherent Processing and Superresolution Technique of Multi-Band Radar Data Based on Fast Sparse Bayesian Learning Algorithm," *IEEE Trans. Antennas Propag.*, vol. 62, no. 12, pp. 6217-6227, Dec. 2014.
- [7] M. J. Gerry, L. C. Potter, I. J. Gupta *et al.*, "A parametric model for synthetic aperture radar measurements," *IEEE Trans. Antennas Propag.*, vol. 47, no. 7, pp. 1179-1188, Jul. 1999.
- [8] H. Liu, B. Jiu, F. Li, and Y. Wang, "IEEE Attributed Scattering Center Extraction Algorithm Based on Sparse Representation With Dictionary Refinement," *IEEE Trans. Antennas Propag.*, vol. 65, no. 5, pp. 2604-2614, May 2017.
- [9] Yu, Y., Liu, Y., Yan, G, "Encoding Theory and Application of Genetic Algorithm," *Computer Engineering and Applications*, vol. 43, no. 3, pp. 86-89, 2006.